Chemical composition and physico-mechanical properties of carbonated alkali activated concrete and mortar.

OJEDOKUN, Olalekan <http://orcid.org/0000-0002-9573-4976> and MANGAT, Pal <http://orcid.org/0000-0003-1736-8891>

Journal of Building Engineering 71 (2023) 106480

Contents lists available at ScienceDirect

Journal of Building Engineering

journal homepage: www.elsevier.com/locate/jobe

Chemical composition and physico-mechanical properties of carbonated alkali activated concrete and mortar

Olalekan O. Ojedokun, P.S. Mangat *

Centre for Infrastructure Management, Materials and Engineering Research Institute, Sheffield Hallam University, Sheffield, S1 1WB, UK

ARTICLE INFO

Keywords:
Alkali activated concrete (AAC)
Portland cement concrete (PCC)
Carbonation
Pore chemistry
Alkali content
Phenolphthalein indicator method

ABSTRACT

This paper investigates the influence of CO_2 concentration (ambient and 5%) and duration of exposure on the carbonation, alkali content and pH of alkali activated concrete (AAC) and mortar produced from a ggbs based alkali activated cementitious material (AACM). Depth of carbonation was measured at regular intervals by the standard phenolphthalein indicator test method. The alkali content, mineralogy, and pH of the AAC in its carbonated and non-carbonated zones was determined by XRD, XRF, EDS and pH analysis. The effect of carbonation on physical properties (porosity, shrinkage) and mechanical properties (compressive strength) of alkali activated concrete (AAC) and mortar (AAM) together with their corresponding Portland cement-based specimens (PCC and PCM) was determined.

The results show significantly high pH (between 10 and 10.5) at the carbonated zone of AAC and AAM. The high pH at the carbonated zone of AAC and AAM depicts sufficient alkalinity within the zone to prevent reinforcement corrosion due to carbonation. The alkalis Na^+, K^+, Al^{3+} and Mg^{2+} are more abundant in AAC and AAM which boost its alkalinity relative to the control PCC and PCM. The phenolphthalein test is more sensitive for detecting the carbonation of alkalis $Ca(OH)_2$ and C–S–H which are predominant in PCC and PCM.

The long-term depth of carbonation is lower in AAC than the control PCC under ambient CO_2 exposure, but it is greater under accelerated carbonation (5% CO_2) when kinetically unstable reactions occur, and bicarbonate is also formed. Results on the total drying and carbonation shrinkage, carbonation rate, and compressive strength are also reported which show the dominant influence of porosity of AAC and PCC.

1. Introduction

Alkali activated concrete (AAC), as a construction material, has many attributes over Portland cement concrete (PCC). These include low CO_2 emission and energy demand during production [1,2], high mechanical strength and good pore properties [3,4]. An enhanced understanding of chloride diffusion in AAC is presented in recent publications [5,6], showing higher resistance to chloride induced corrosion of steel reinforcement in AAC [7]. Carbonation of AAC is another potential cause of steel reinforcement corrosion [8,9]. The full potential of AAC cannot be realized until conclusive evidence is available of its corrosion protection properties for the embedded steel reinforcement. Unlike conventional reinforced concrete, design solutions for durable AAC mixes and steel reinforced structures have not been developed.

More knowledge is required on the ingress of CO_2 and its effects on the chemical and mineralogical compositions, alkalinity, mechanical and physical properties (porosity) of AAC, which provide corrosion resistance to steel reinforcement against carbonation.

* Corresponding author.
E-mail address: p.s.mangat@shu.ac.uk (P.S. Mangat).

https://doi.org/10.1016/j.jobe.2023.106480
Received 20 December 2022; Received in revised form 3 April 2023; Accepted 3 April 2023
Available online 5 April 2023

Field applications of AAC will be restricted until full confidence is provided in its corrosion protection of steel reinforcement. It is noteworthy to mention the example of existing steel reinforced AAC structure which are still durable after 60years in service [10].

Standard durability test methods, such as the phenolphthalein test, are commonly adopted for AAC to provide information on the carbonation front [11,12]. This test method is affected by the chemical and physical interactions between the AAC gel matrix and CO_2 [13,14]. There is not sufficient information in literature about the impact of these interactions to elucidate the validity of the phenolphthalein test for monitoring carbonation of AAC. A good understanding of the chemical nature of the carbonation products in AAC is required for developing a suitable carbonation test method.

CO_2 concentration of the environment and duration of exposure are two major factors that affect the carbonation of AAC and the resulting corrosion of reinforcement affecting the structural performance of steel reinforced AAC. For example, accelerated carbonation testing of AAC and AAM by exposure to high CO_2 concentrations in the laboratory, produced an overestimation of its actual degradation in service life [15]. The authors [15] suggested that accelerated carbonation changed the AAC and AAM pore solution equilibria, leading to a higher apparent carbonation rate compared to carbonation under natural conditions. The complex pore chemistry of AAC produced due to its different binder constituents is likely to alter the precision of experimental results obtained from test standards developed for conventional PCC [15].

Published results provide an inconsistent comparison on the carbonation of AAC with PCC. For example, high depths of carbonation were recorded for silicate-activated blast furnace slag concrete and mortar compared with PCC and PCM under accelerated carbonation conditions [10–20% CO_2 and 70% R.H.] [16]. This observation agrees with Bernal et al. [15] when AAC is exposed to high CO_2 concentration resulting in overestimation of its actual degradation in service life. Other studies show that the depth of carbonation of alkali activated blast furnace slag concrete and mortar is comparable to those of PCC and PCM [17–19]. The authors [17–19] concluded that the refinement of the pore structure of alkali activated blast furnace slag concrete and mortars induced by high relative humidity is responsible for its resistance to carbonation. However, a high relative humidity above 70% when used for the accelerated carbonation test would slow the diffusion of CO_2 within the concrete and mortar matrices and invalidate carbonation test results. Disparities in the carbonation test results of AAC are likely to be linked more with the level of CO_2 concentrations and duration of exposure of the concrete. This paper aims to evaluate the performance of AAC, AAM and PCC, PCM under short and long-term exposures at high and low concentrations of CO_2.

The influence of carbonation on the pore fluid chemistry and pore properties of PCC and PCM is well documented while limited knowledge is available for AAC and AAM [20,21]. The carbonation of AAC and AAM will depend largely on its pore fluid chemistry. The effect of spraying phenolphthalein solution on a carbonated concrete surface indicates the depletion of $Ca(OH)_2$ [11] which is predominantly present in PCC but the geopolymerization reactions in AAC yield less $Ca(OH)_2$ [22]. However, the alkalinity of AAC is not only supplied by $Ca(OH)_2$, but also by other alkali boosters in the pore fluid chemistry of AAC [7,23]. The impact of carbonation on the pore fluid chemistry and alkalinity of AAC and AAM will be investigated in this paper to elucidate their inter-relationship.

The rate of carbonation in concrete is a slow process which sometimes takes years to manifest. Concrete structures in large cities are susceptible to carbonation due to human activities involving high emissions of CO_2, up to 1% by volume of air [24]. The carbonation chamber used in the laboratory for accelerated testing in this investigation was maintained at 5% CO_2 concentration, 65% relative humidity and a temperature of 20 °C to achieve the optimum rate of carbonation in both AAC and the control PCC within the project period. Powdered samples of concrete and mortars were collected from two zones "carbonated" and "non-carbonated" as determined by the phenolphthalein test method. The samples were analyzed to investigate and determine the effect of carbonation on their alkalinity and pH, including the influence of coarse aggregates.

This paper presents findings on the influence of CO_2 ingress on the alkalinity, chemical and mineralogical compositions of AAC, AAM and the control PCC, PCM by studying zones which are carbonated and non-carbonated as determined by the phenolphthalein indicator test method [11,12]. Studies on the carbonation rates and shrinkage of AAC and PCC over long period of exposure (up to 2113 days) to high and low CO_2 concentration were carried out, followed by determining the total drying and the net carbonation shrinkage. Investigation on the long-term effect of carbonation on mechanical and microstructural properties of AAC, PCC and their mortars were also carried out and their relationship with porosity was determined.

The results show that carbonation process in AAC can be managed equally well as in conventional concrete, despite basic differences in their chemical products of carbonation. Therefore, its use for large scale construction is not prevented by carbonation concerns. This paper will facilitate further research on developing the tools for achieving its impact, such as design guidelines for durable AAC mixes and structures, including corrosion tests on steel reinforced AAC.

2. Materials and methods

2.1. Materials and mixes

Details of AAC and AAM mixes and the control PCC and PCM mixes are given in Table 1. AAC and AAM 1, 2 and 3 relate to high, medium and low grades of strength respectively, representing different pore properties [3] and, therefore, with varying rates of CO_2 diffusion. The control PCC and PCM mixes have similar design strength as AAC 3 and AAM 3 respectively.

The alkali activated and control samples were produced from ground granulated blast furnace slag (GGBS) and ordinary Portland cement CEM 1 of grade 42.5R [25] respectively. Chemical compositions of Portland cement and GGBS binders are shown in Table 2. The aggregates used were 10 mm uncrushed gravel, 6 mm limestone and a medium grade sand of 80% particle size passing 1 mm sieve size.

The AAC and AAM binders were activated with a sodium silicate solution of molarity 6.5 mol/L and modulus 2% together with NaOH of molarity 4.8 mol/L. The activators used in AAC and AAM 1, 2 and 3 mixes were diluted with water at 0%, 3.88% and 7.76%

Table 1
Mix composition of AAC and AAM 1, 2, 3 and the control PCC and PCM.

	Mix	Binder Content (Kg/m^3)	Fine Agg. (Kg/m^3)	Coarse Agg. (Kg/m^3)		Liquid/Binder Ratio	Activator Dilution (%)	R42	SRA	Porosity %
				10 mm Gravel	6 mm Limestone			(Kg/m^3)		
Concrete	AAC 1	600	432	700	377	0.47	0	1.2	3	–
	AAC 2	600	432	700	377	0.47	3.88	1.2	3	–
	AAC 3	600	432	700	377	0.47	7.76	1.2	3	–
	Control PCC	480	624	694	372	0.47(w/c)	–	–	–	–
Mortar	AAM 1	600	1300	–	–	0.5	0	1.2	3	4.64
	AAM 2	600	1300	–	–	0.5	3.88	1.2	3	6.67
	AAM 3	600	1300	–	–	0.5	7.76	1.2	3	10.56
	Control PCM	600	1300	–	–	0.5(w/c)	–	–	–	14.02

*R42 is the retarder; SRA is the shrinkage reducing admixture.

Table 2
Chemical and physical properties of binders and aggregates.

Chemical properties	SiO_2	Al_2O_3	Fe_2O_3	CaO	MgO	K_2O	Na_2O	TiO_2	P_2O_5	MnO	SO_3	LOI
PC (mass %)	11.1	8.35	3.16	64.2	2.09	1.19	0.227	1.88	2.01	2.14	3.64	–
GGBS (mass %)	28.6	12.4	5.70	42.3	6.1	0.8	0.4	1.78	<0.1	0.3	0.08	–
Limestone (mass %)	8.19	0.89	0.48	51.4	1.27	0.15	0.1	–	–	–	0.11	37.4
Gravel (mass %)	87.5	6.1	1.62	0.28	0.03	–	2.08	–	–	–	0.06	2.33
Sand (mass%)	91.7	3.89	1.1	0.8	0.2	0.01	0.16	–	–	0.78	–	1.36

Physical properties	PC	GGBS	Limestone	Gravel	Sand
Specific gravity (g/cm^3)	3.15	2.79	2.69	2.65	2.63
Specific surface area (m^2/g)	0.39	0.42	0.83	0.76	0.67
pH	10.8	11.1	12.8	8.1	7.95
% Absorption	–	–	0.4	0.48	1.20
Initial setting (mins)	128	126	–	–	–
Final setting (mins)	364	362	–	–	–

respectively as shown in Table 1, to optimize workability and determine the effect of activator dilution on carbonation. Liquid/binder ratios of 0.47 and 0.5 were used in the concrete and mortar mixes respectively. The AAC and AAM mixes contained 0.5% by binder weight of a shrinkage reducing admixture (SRA) made from Alkyl-ether and 0.2% by binder weight of retarder R42 made from a blend of high grade polyhydroxycarboxylic acid derivatives. The shrinkage reducing admixture (SRA) enhances workability while the retarder (R42) increases the setting time of AAC concrete and mortars. These admixtures were required for the AAC mixes at the activator/binder ratio of 0.47 (Table 1). The workability and setting time of PC concrete mixes was satisfactory at water/cement ratio of 0.47 (Table 1) and did not require SRA and R42.

2.2. Specimen preparation

The fresh AAC, PCC and corresponding mortars were mixed in a 150 kg capacity Cretangle mixer in accordance with BS EN 206:2013 + A1:2016 standard [25]. Two types of specimens were produced for the carbonation investigation. The first were prisms of 300 mm × 75 mm x 75 mm dimensions, which were used to determine the carbonation shrinkage and the rate (depth) of carbonation in AAC and PCC mixes only. The second were cylinders of 50 mm diameter by 60 mm depth, which were used to investigate the effect of carbonation on the alkalinity of both the concrete and mortars of the alkali activated and control mixes.

2.2.1. Specimens for carbonation rate

A total of sixteen concrete prisms (75 mm × 75 mm x 300 mm) were prepared in accordance with BS 1881–210:2013 [26] for the carbonation investigation. The concrete prisms were demoulded at 24 h after casting and then cured in water at 20 ± 2 °C for 27-days. This was followed by dry curing for 42days at 65% R.H. and 20 ± 2 °C until a minimal change in unit weight of less than 0.2% was achieved during a 24-h period. Two coats of bitumen paint were applied to two opposite longitudinal faces (75 mm × 300 mm) and ends of each prism specimen, leaving two opposite longitudinal faces uncoated to allow uni-directional CO_2 diffusion without any interaction of the carbonation fronts from the two opposite faces (samples shown in the carbonation chambers, Fig. 1). The specimens were then placed inside the carbonation chamber and exposed to 5% CO_2 concentration at 60 ± 5% R.H. and 20 ± 2 °C up to 2113-days (Fig. 1a). The depths of carbonation were determined by using the phenolphthalein indicator method at 28, 55, 90, 145, 327 and 2113 days of CO_2 exposure. Four prisms for each mix were used to determine the rate of carbonation.

2.2.2. Specimens for shrinkage of concrete

Sixteen concrete prisms (75 mm × 75 mm x 300 mm) were produced in accordance with BS 1881–210:2013 [26] to investigate carbonation shrinkage in both AAC and PCC. The specimens were demoulded 24hrs after casting and demec points applied on two-

Fig. 1. Concrete and mortar specimens (a) exposed to 5% CO_2 concentration in accelerated carbonation chamber (b) cast in cylindrical plastic moulds and (c) with self-adhesive tape fixed at the base of cylindrical moulds.

parallel longitudinal (75 mm × 300 mm) side faces (relative to the casting position) at a gauge length of 200 mm. The specimens were cured in water (20 ± 2 °C) for 7 days in accordance with [27]. Eight concrete specimens were exposed to 5% CO_2 concentration at 60 ± 5% R.H. and 20 ± 2 °C temperature in the carbonation chamber for 80 days (Fig. 1a) while the remaining eight samples were left in laboratory air (drying shrinkage) at 0.4% CO_2 concentration at 60 ± 5% R.H. and 20 ± 2 °C temperature. The readings of carbonation shrinkage were taken and recorded at regular intervals. No bitumen paint was applied to the faces of the prism specimens, to allow free CO_2 diffusion from all faces.

The absolute carbonation shrinkage was calculated by applying equation (1).

$$Dc = Dt - Dd \quad (1)$$

where.

Dc = absolute carbonation shrinkage
Dt = total shrinkage of specimens exposed in carbonation chamber at 5% CO_2 concentration, 20 ± 2^{0}C and *60 ± 5% R.H*
Dd = Drying shrinkage of specimens exposed in the laboratory air at 0.4% CO_2 concentration, 20 ± 2 °C and 60 ± 5% R.H.

2.2.3. Concrete and mortar specimens for pH analysis

Concrete and mortar specimens were cast into non-standardized cylindrical plastic moulds of 50 mm diameter x 60 mm depth as shown in Fig. 1b. The specimens were produced and cured with all faces covered with the plastic mold except the top cast face to allow for CO_2 ingress from the top cast face only. This also allows the collection of powder at two sections (carbonated and non-carbonated) within the same test samples for pH analysis as detailed in Section 2.3.1.

Self-adhesive bitumen tape was fixed at the bottom of the mold before casting to prevent concrete from pouring out (Fig. 1c). The fresh concrete and mortar in the cylindrical moulds was compacted in two layers on a vibrating table. The specimens were covered with polythene sheets and cured in the laboratory air (20 ± 2 °C, 65% R.H.) for 24hrs after casting. This was followed by curing in water at 20 ± 2 °C for 27days and then dry curing for 42days at 65% R.H. and 20 ± 2 °C until a minimal change in unit weight of less than 0.2% was achieved during a 24-h period. The specimens were then placed inside the carbonation chamber and exposed to 5% CO_2 concentration at 60 ± 5% R.H and 20 ± 2 °C for 327days (Fig. 1a). They were retained in their moulds throughout the period after casting, leaving only the top face exposed to diffusion of the 5% CO_2 concentration in the chamber for 327days.

A total of twenty-four specimens were produced for both the concrete and mortar, representing six specimens per each mix in Table 1. The specimens were grouped into two after the CO_2 exposure for 327days. The first group were used to establish the carbonated boundaries using the phenolphthalein indicator method [11], by spraying phenolphthalein solution on the CO_2 exposed top surfaces of the specimens For the second group, no phenolphthalein solution was sprayed on the CO_2 exposed surfaces of the concrete and mortar specimens. The depth of carbonation profile obtained in the first group was transferred (plotted) on the surfaces of their corresponding specimens in the second group. Powder samples for pH analysis and chemical analysis for alkali content were collected from the plotted carbonated and non-carbonated zones in the second group of concrete and mortar specimens as shown in Figs. 2 and 3. The procedure was carried out to investigate the influence of carbonation on their pore chemistry.

2.3. Test procedure

2.3.1. Powder collection

Specimens within the cylindrical plastic moulds were removed from the carbonation chamber after 327days of accelerated CO_2 exposure. They were de-moulded and split longitudinally into two halves as shown in Fig. 2. The splitting tensile strength test procedure was adopted to break the cylindrical specimens into the two longitudinal halves. The carbonated boundaries were determined by

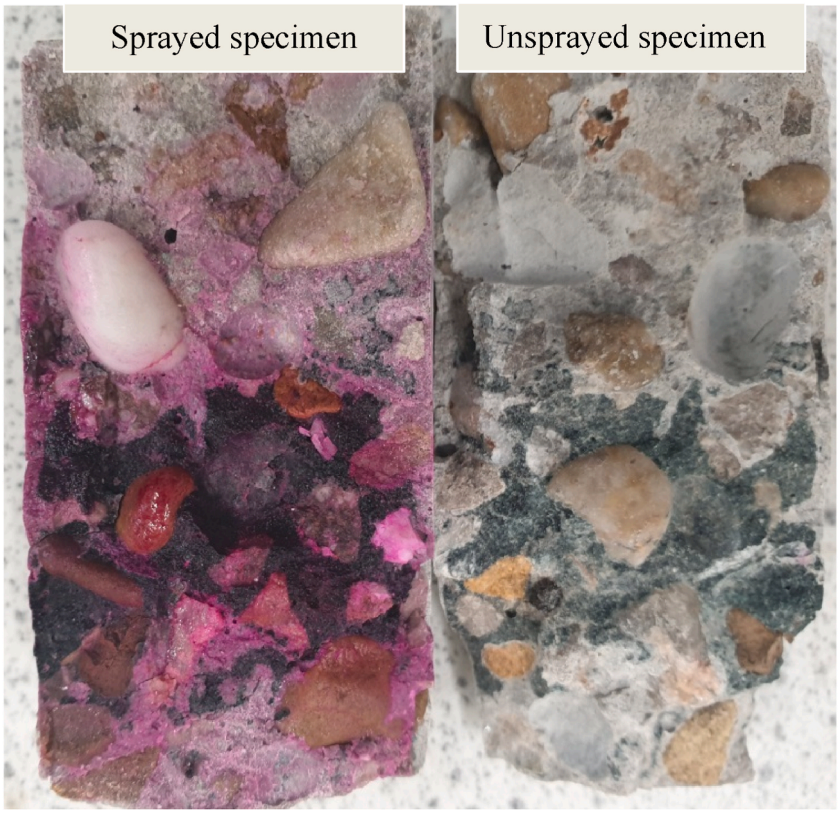

Fig. 2. Specimen split into two longitudinal halves, with one half sprayed with phenolphthalein solution.

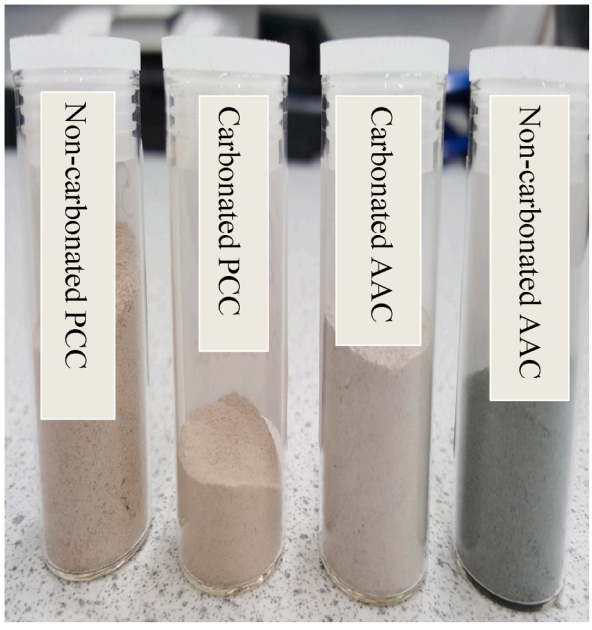

Fig. 3. AAC and PCC powder in air-proof plastic vials.

spraying phenolphthalein solution on the exposed (split) surface of one broken half of the cylinder according to the carbonation test method [11]. However, phenolphthalein was not applied to the surface of the other half (unsprayed specimen) as shown in Fig. 2.

The depth of carbonation profile obtained from the sprayed specimen was marked on the unsprayed specimen. Representative chunks of concrete from the carbonated and non-carbonated zones were then carefully chiseled out from the unsprayed specimen. These were ground to powder (including the coarse aggregate) and passed through a 150 μm sieve to obtain a fine powder of the carbonated and non-carbonated zones (Fig. 3). The same procedure was adopted for the mortar specimens to obtain powder from the

crushed carbonated and non-carbonated mortar chunks. These procedures were performed on six specimens for each concrete and mortar mix to obtain adequate chunks for grinding into their respective powders. The alkali content and pH analysis were performed on both the concrete powder passing and retained on 150 μm sieve.

2.3.2. pH analysis

The ex-situ leaching method of concrete testing [28] was adopted to obtain solutions for the pH analysis of AAC, PCC and mortar samples. This was carried out by dissolving 5 g of powder samples in distilled water at a liquid/solid ratio of 1:1 in an air-tight plastic vial. The solution was shaken thoroughly for 2mins to ensure a homogenous mix and then left undisturbed for 5mins to allow for leaching. This procedure was carried out on both carbonated and non-carbonated powder samples. The powder solution was then filtered to remove all particles. A double junction electrode connected to a 3-in-1 benchtop meter was dipped into the filtered solution to measure its pH. This device measures pH ranging from 0.00 to 14.00 of sample volumes as small as 0.2 mL with an accuracy of ± 0.01.

2.3.3. XRD and XRF

The carbonated and non-carbonated powder samples of AAC and PCC were tested using a Philips X-Pert X-ray diffractometer operating with a Cu Kα radiation source (40 KV and 40 mA, wavelength $\lambda = 0.154056$ nm [6.07×10^{-9} in.]). XRD analysis of powder samples from the carbonated and non-carbonated zones were performed by scanning from 5^0 to 50^0 at an angle of 2Θ; the scan step size was 0.016711 with a counting time step of 0.1 s. A Niton XL3t portable XRF spectrometer was used to analyze carbonated and non-carbonated powder samples of AAC and PCC. This gave information on the chemical elements present, showing elements from Mg and above in the periodic table.

2.3.4. Scanning electron microscopy (SEM/EDS)

FEI NOVA 200 NanoSEM with high spatial resolutions of 1.5–2.0 nm (15–30 KV) compatible with both high vacuum and low-pressure environments was used to investigate the composition phases in both AAC and PCC. The powder samples were impregnated with a low viscosity epoxy which was cured to harden in air for 24hrs. The hardened epoxy was polished off to reveal the surface of specimens. Specimens were carbon coated prior to SEM/EDS analysis. Microanalysis of the oxides was performed on the carbonated and non-carbonated phases in AAC and PCC.

2.3.5. Compressive strength

Compressive strength test of mortar and concrete mixes in Table 1 were performed after curing in water for 28days and long-term CO_2 exposure (2113days) to ambient (0.4% CO_2) and high concentrations (5% CO_2) curing. The compressive strength tests on the cubes were conducted in accordance with *BS EN 12390-3:2009* [29]. The density of the cubes was determined according to BS EN 12390–7:2009 [30]. An average of three cube ($75 \times 75 \times 75$ mm) were used to determine the compressive strength and density of each mortar and concrete mix. A loading rate of 3 MPa/min was applied during the compression testing and a post peak of 30% failure load was programmed into the compression machine to prevent complete disintegration of the crushed specimen.

3. Results and discussion

3.1. Mineralogical and chemical characterization

3.1.1. XRD and XRF

The XRD diffractograms showing peaks of mineral compounds present in the carbonated and non-carbonated samples of AAC and PCC are presented in Fig. 4. The assigned numbers on the graph are peaks where these minerals are observed, and their legends are shown below. PCC shows peaks of Calcium silicate hydrate CSH, Calcite, Ettringite, Gypsum and Portlandite. The mineral compounds present in AAC are C-(N)-A-S-H, Nahoclite ($NaHCO_3$), Albite, Sodium, alumina, silicate and quartz.

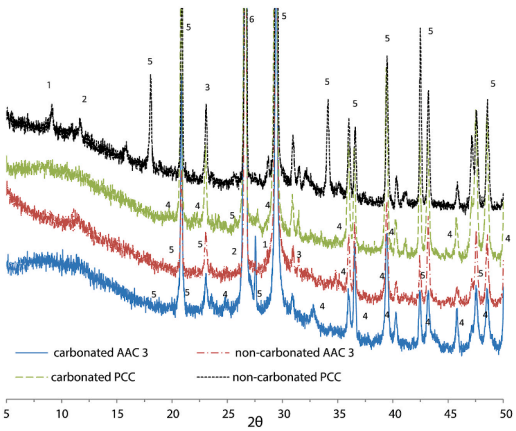

Fig. 4. X-ray diffraction patterns of carbonated and non-carbonated samples of AAC and PCC at 327days CO_2 exposure.

The decomposition due to carbonation of Ettringite $Ca_6Al_2(SO_3)_4(OH)_{12}.26H_2O$, Gypsum $CaSO_4.2H_2O$, Calcium silicate hydrate C–S–H and Portlandite $Ca(OH)_2$ in PCC is observed to produce dominant peaks of Calcite $CaCO_3$. There are cation exchanging reactions of Ca^{2+} from the gel matrix of PCC with carbonate ion from the carbonated aqueous pore solution resulting in the dominant calcium-based carbonates [31] in Fig. 4. In the case of AAC, the exchanging cation is predominantly Na^+ which reacts with the aqueous solution saturated with carbonate ion to form Nahoclite ($NaHCO_3$). The high sodium content in AAC is supplied by the alkali activator containing sodium silicate solution of molarity 6.5 mol/L and modulus 2% together with NaOH of molarity 4.8 mol/L.

In addition, the Na-carbonate products formed in AAC are arguably influenced by the conditions of carbonation which produce three Na-carbonate products namely natron ($Na_2O_3.10H_2O$), Nahoclite ($NaHCO_3$) and gaylussite ($Na_2Ca(CO_3)_2.5H_2O$) in carbonated slag based AAC samples [31]. Natron ($Na_2O_3.10H_2O$) is most likely to form at 21 ± 2 °C under CO_2 concentration of less than 0.04%. Nahoclite ($NaHCO_3$) forms at CO_2 concentration greater than 0.2% which agrees with the data in Fig. 4 for AAC exposed to 5% concentration of CO_2. Gaylussite ($Na_2Ca(CO_3)2.5H_2O$) occurs at temperature below 250 °C during dehydration of double salts such as pirssonite [31].

The PANlytical quantification by applying Rietveld method (Malvern Panalytical) to the data of AAC and PCC samples is shown Table 3. The Rietveld method fits a calculated profile to experimental data by applying the least squares approach to quantify the chemical products present in the AAC and PCC samples. The chemical products are expressed as percentage weight in Table 3. The differences in the chemical elements present in non-carbonated and carbonated samples of AAC 1, 2, 3 and PCC are also presented in Table 3.

Table 3 shows a reduction in the quantity of calcium oxide present in both carbonated AAC and PCC samples relative to their non-carbonated samples.

The percentage loss of calcium oxide content in the carbonated samples of AAC 1, 2, 3 and PCC are 12.55%, 17.03%, 20.43% and 10.58% respectively as shown in Table 3. A significant depletion of Ca^{2+} content is shown in AAC 3 (20.43%) particularly in relation to PCC (10.58%) of similar strength grade (Fig. 8). The low depletion rate of Ca^{2+} content in PCC is synonymous to its initial high calcium content in non-carbonated samples as a result of combined Portlandite $Ca(OH)_2$ and C–S–H present within its matrix as shown in Fig. 4. The only source of calcium in non-carbonated AAC is the C–S–H within its matrix (Fig. 4) leading to higher depletion of calcium oxide after carbonation relative to PCC.

In addition, the calcium oxide contents of GGBS and PC binders are 42.3% and 64.2% respectively (Table 2). As such, it is not surprising to observe lower percentage of calcium oxide in AAC concrete. This is further supported by more peaks of Nahoclite ($NaHCO_3$) in AAC than calcite ($CaCO_3$) in PCC as shown in Fig. 4. The other phases detected in the non-carbonated AAC concrete are albite, sodium aluminium silicate, CSH and quartz. The predominant peaks observed in the carbonated AAC concrete are Nahoclite and quartz while other compounds are in minor traces which could not be detected by XRD. Predominant compounds in the carbonated PCC are calcite and quartz which are produced when Ettringite, Gypsum, CSH and Portlandite, which are rich in calcium hydrates, react with carbonic acid to form Calcite. Minor traces of Ettringite, Gypsum, CSH and Portlandite are also present in the carbonated PCC. The relationship between the depletion of calcium oxide and carbonation depths for AAC and PCC will be detailed in section 3.2.3.

Alkali activator concentrations in AAC 1, 2 and 3 show significant impact on the depletion of Ca^{2+} content as seen in Table 3. AAC 3 with the lowest activator molarity had the highest depleted Ca^{2+} content (20.43%) than AAC 1 and 2, due to higher porosity, lowest pH and alkalis, which is discussed in the next section.

3.1.2. Energy dispersive spectrometer (EDS)

The various alkalis present in carbonated and non-carbonated samples of AAC and PCC were determined by Energy dispersive spectrometer (EDS) mapping and the data are shown in Table 4. The binder gel comprised mainly oxides of carbon, calcium, silica, sodium, alumina, potassium and magnesium. The pH of the powder solution of carbonated and non-carbonated samples of AAC and PCC and the summation of alkali contents (Ca^{2+}, Na^+, K^+, Al^{3+} and Mg^{2+}) are also shown in Table 4.

Table 3
Chemical products in carbonated and non-carbonated AAC and PCC at 327days CO_2 exposure.

	CaO	Na_2O	MgO	Al_2O_3	SiO_2	SO_3	K_2O	P_2O_5	TiO_2	MnO	Fe_2O_3
non-carbonated AAC 1 (%)	51.63	4.18	5.52	12.15	20.93	1.85	1.01	0.14	0.39	0.63	0.88
carbonated AAC 1 (%)	39.08	2.83	2.99	8.12	42.72	0.64	0.92	0.14	0.29	0.44	1.14
[a]difference AAC 1 (%)	12.55	1.35	2.53	4.03	−21.79	1.21	0.09	0	0.1	0.19	−0.26
non-carbonated AAC 2 (%)	51.36	4.18	5.65	11.86	22.22	2.02	0.71	0.08	0.30	0.42	0.63
carbonated AAC 2 (%)	34.33	2.83	3.11	7.84	48.49	0.81	0.62	0.08	0.20	0.23	0.89
*difference AAC 2 (%)	17.03	1.35	2.54	4.02	−26.27	1.21	0.09	0	0.1	0.19	−0.26
non-carbonated AAC 3 (%)	48.91	4.48	4.85	13.23	23.33	1.65	1.19	0.10	0.41	0.60	1.34
carbonated AAC 3 (%)	28.48	3.14	2.32	9.21	52.86	0.43	1.10	0.10	0.32	0.41	1.60
*difference AAC 3 (%)	20.43	1.34	2.53	4.02	−29.53	1.22	0.09	0	0.09	0.19	−0.26
non-carbonated PCC (%)	55.03	0.0	0.97	3.67	34.48	0.79	1.00	0.11	0.13	0.0	3.55
carbonated PCC (%)	44.45	0.0	1.17	4.50	44.82	0.53	1.08	0.11	0.12	0.20	2.97
*difference PCC (%)	10.58	0.0	−0.2	−0.83	−10.34	0.26	−0.08	0.0	0.01	−0.2	0.58

[a] Difference is: CaO non-carbonated minus CaO carbonated.

Table 4
Alkali content and pH of carbonated and non-carbonated samples of AAC and PCC at 327days CO_2 exposure.

	C	Ca^{2+}	Si	Ca^{2+}/Si	Na^{+}	K^{+}	Al^{3+}	Mg^{2+}	Alkalis	pH
carbonated AAC 1 (%)	10.4	12.8	20.4	0.63	1.7	0.3	3.1	1.4	19.3	10.46
non-carbonated AAC 1 (%)	6.5	15.1	22.6	0.67	4.0	0.4	3.8	1.5	24.8	13.58
carbonated AAC 2 (%)	11.5	12.1	20.6	0.59	1.8	0.4	2.8	1.4	18.5	10.37
non-carbonated AAC 2 (%)	8.2	14.3	21.8	0.66	4.1	0.5	3.3	1.5	23.7	13.48
carbonated AAC 3 (%)	13.7	9.2	20.7	0.44	1.6	0.4	2.4	1.5	15.1	10.25
non-carbonated AAC 3 (%)	10.2	12.4	21.2	0.58	4.2	0.5	3.0	1.6	21.7	13.33
carbonated PCC (%)	23.0	14.1	16.8	0.84	0.2	0.2	0.6	0.2	15.3	9.56
non-carbonated PCC (%)	14.4	17.0	18.0	0.94	0.2	0.4	1.0	0.3	18.9	12.82

The depletion of Ca^{2+} due to carbonation is highest in AAC 3 concrete from 12.4% to 9.2% (3.2%) followed by PCC which decreased from 17.0% to 14.1% (2.9%) (Table 4). The summation of Ca^{2+}, Na^{+}, Al^{3+}, K^{+} and Mg^{2+} alkalis is similar in carbonated AAC 3 (15.1%) and PCC (15.3%). However, significantly higher amounts of total alkalis Ca^{2+}, Na^{+}, Al^{3+} and Mg^{2+} are observed in the carbonated AAC 1 (19.3%) and 2 (18.5%) than PCC (15.3%). The alkalis (Na^{+}, K^{+}, Al^{3+} and Mg^{2+}) are considerably greater in AAC than PCC and contribute significantly to the alkalinity of pore fluid in AAC (section 3.1.3). For example, the higher total alkali contents in the carbonated zone of AAC 1 (19.1%) and 2 (18.5%) than PCC (15.3%) also show correspondingly higher pH values in AAC 1 and 2 (10.46 and 10.37 respectively) than PCC (9.56), which is discussed further in section 3.1.3.

The molarity of alkali activator contributed significantly to the amount of alkalis present in AAC. AAC 1 has the maximum overall alkalis and pH compared to AAC 2 and 3. In addition, the reaction kinetics in AAC 1 are faster than AAC 2 and 3 due to its highest molarity which impedes the depletion of alkali content. It was observed that at low Ca/Si ratio, the negative charge of the CSH surface is compensated by N^{+}, K^{+} and Mg^{2+} [32]. This occurs by replacing Ca^{2+} in the negative surface charge of silicate chain as a result of de-protonation from -SiOH to –SiO– sites [33]. The Ca/Si ratios of carbonated and non-carbonated samples of AAC 1, 2 and 3 are lower than PCC. For example, Ca/Si ratios of carbonated and non-carbonated samples of AAC 3 are 0.44 and 0.58 respectively (Table 4) compared with the corresponding values for PCC of 0.84 and 0.94. The higher N^{+}, Al^{3+}, K^{+} and Mg^{2+} content in AAC 3 compensates for its low Ca/Si ratio thus resulting in higher pH than PCC as shown in Table 4. A similar trend is observed in AAC 1 and 2 which have lower Ca/Si ratios than PCC.

The carbon content, C, which is integral to carbonation ($CaCO_3$) is much higher in carbonated samples of PCC (23.0%) than carbonated AAC 1, 2 and 3 having 10.4%, 11.5% and 13.7% respectively as shown in Table 4. Fig. 5 shows the carbon mapping of carbonated samples of AAC and PCC determined by EDS. Distinct carbon mapping is observed on the hydration products formed in the space between aggregates in PCC whereas the carbon mapping on the geopolymerisation products formed in the space between aggregates in AAC 3 concrete is faint. The carbon content, C, reduces the alkalis and pH values of AAC and PCC as shown in Table 4. The highest carbon content observed in the carbonated PCC (23.0%) resulted in the lowest values of alkali (15.3%) and pH (9.56). Conversely, the carbon content in carbonated AAC 1 (10.4%), AAC 2 (11.5%) and AAC 3 (13.7%) shows alkali values of 19.3%, 18.5% and 15.1% by weight respectively and a corresponding pH value of 10.46, 10.37 and 10.25. This clearly shows a negative impact of carbon content, C, on alkalis and pH values.

3.1.3. pH

Fig. 6 shows the pH of powder solutions extracted from the carbonated and non-carbonated samples of both concrete and mortar mixes of alkali activated and the control Portland cement mixes given in Table 1. The procedure for obtaining concrete and mortar powdered samples is detailed in section 2.3.1.

The pH values of solutions extracted from the carbonated zones of all mixes are above the pH threshold of 9 except for PCM mortar as shown in Fig. 6. PCM mortar has significantly lower pH than 9 which indicates loss of alkalinity [34,35]. The pH values for AAC 1,

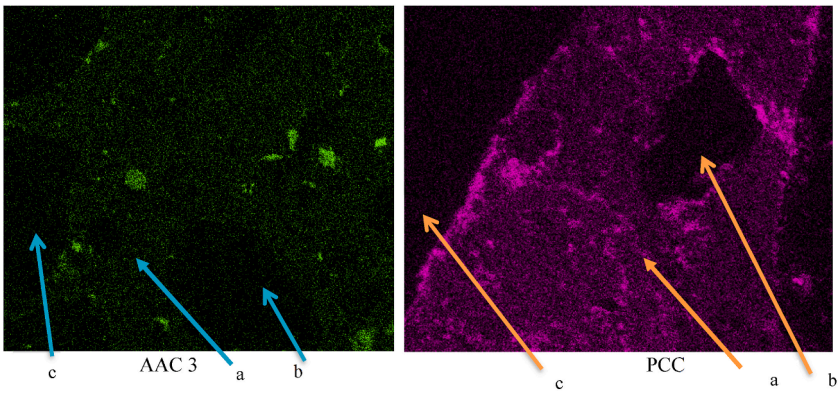

Fig. 5. EDS mapping of carbon content in AAC 3 and PCC at 327days CO_2 exposure showing (a) binder gel matrix (b) coarse aggregate (c) carbon.

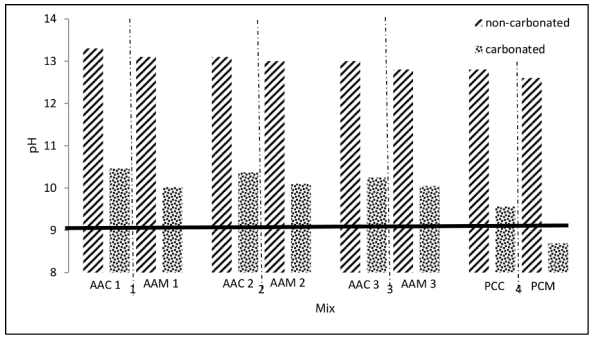

Fig. 6. pH of AAC and PC concrete and mortar after 327days exposure to 5% CO_2.

2, 3 and PCC are 10.46, 10.37, 10.25 and 9.56 respectively. The corresponding values of pH for mortars are 10.02, 10.1, 10.05 and 8.69 respectively. The extent of carbonation in PCC is measured by spraying phenolphthalein solution on its surface, which is an indirect method of detecting depletion of calcium oxide in PCC [26]. The test is reliable for PCC since its calcium content is predominantly responsible for its alkalinity. However, greater amounts of other alkalis (Na^+, K^+, Al^{3+} and Mg^{2+}) in AAC, shown in Table 4, contribute more to its alkalinity under carbonation than Ca^{2+}. The influence of activator dilution on the pH of powder solution from the carbonated and non-carbonated zones of AAC concrete and AAM mortar is shown in Fig. 7. The activator solution of AAC and AAM is also a source of alkalinity in its pore solution [36].

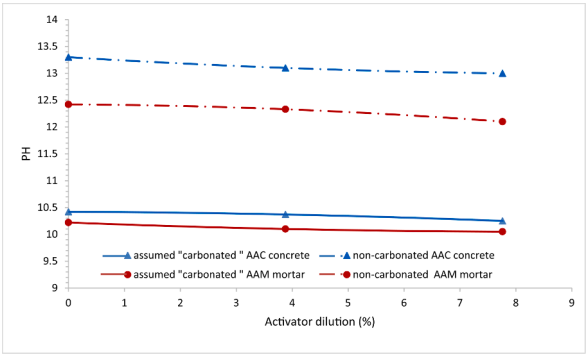

Fig. 7. Influence of activator dilution on pH of AAC and AAM after 327days of CO_2 exposure.

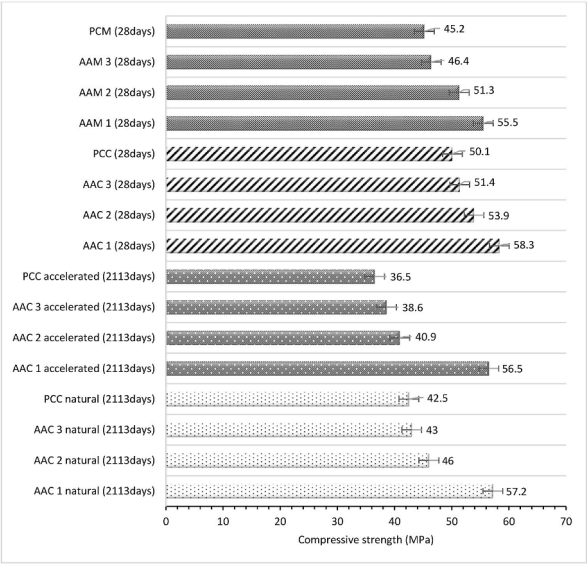

Fig. 8. Compressive strengths of AAC and PCC exposed to accelerated carbonation and natural curing conditions.

Generally, loss of pH caused by carbonation is of great concern because of its impact on reinforcement corrosion. The pore solution pH of carbonated AAC specimens is above the alkaline threshold of 9 (Fig. 6) which will prevent carbonation-initiated corrosion of reinforcing steel [7,8,37].

AAC exposed to ambient CO_2 concentrations will retain higher alkalinity than under accelerated carbonation. This is because the pore chemistry of AAC exposed to CO_2 concentrations above 1% produces bicarbonate contents with higher pH compared with carbonate contents produced under natural CO_2 concentration [30]. The study carried out by Ref. [38] on alkali activated concrete under natural exposure after 8years showed a pH of 10.5 at the carbonated zones. Further research is needed to elucidate the pH threshold value for AAC, including the threshold for reinforcement corrosion under service conditions [18]. pointed out the lack of information in literature on carbonation of AAC in the absence of chlorides.

The pH of powder solutions decreases with increasing activator dilution for both the zones identified by the phenolphthalein test as "assumed carbonated" and non-carbonated in Fig. 7. This is caused by the reduction of alkali elements in the mixes with higher dilution as shown in Table 3. The pH of mortars is lower than their corresponding concrete powders. This difference is due to the release of alkali content from the coarse aggregate in the mix. PCC which had the highest aggregate content of 70.4% compared with 63% for AAC (Table 1) shows the maximum difference (Fig. 7). The pH (9.56) of PCC would have been lower if its aggregate content was the same as AAC. Research carried out by Yinghong [39] shows leaching of alkali content and an increased pH of the pore solution caused by an open graded recycled coarse aggregate. This resulted in a lower rate of carbonation.

3.2. Carbonation and mechanical properties

3.2.1. Workability and compressive strength

The slump test results for fresh AAC 1, 2, 3 and PCC are 30, 45, 70 and 75 mm respectively. The lower workability (slump) for AAC compared with PCC is due to the sticky nature of silicate present in AAC. However, AAC 3 and PCC have similar workability due to reduced silicate content in the activator of AAC 3 (7.76% activator dilution). The densities of AAC and PCC at 28-days age are between 2.24 and 2.45 g/cm^3. The corresponding values for the mortar are 2.07–2.15 g/cm^3.

Fig. 8 shows compressive strengths of AAC 1, 2, 3 and PCC exposed to 2113days of accelerated carbonation (5% CO_2) and natural (laboratory air) curing. The 28-day compressive strengths of AAC 1, 2, 3 and PCC and their corresponding mortar cured in water (20 $\pm$ 2 °C) is also presented in Fig. 8. Error bars representing the standard deviation from the mean value of three tests per mix are included in the graph.

AAC 1 and 2 mixes had greater strength than PCC. The 28-day strength of AAC3 and PCC, under wet curing, is similar (within 2.5%) as is the workability. Therefore, PCC provides the control specimen for AAC 3 under the standard quality control criteria for concrete. The two mixes also have the same liquid/binder and water/cement ratio of 0.47 and 0.50 for concrete and mortar respectively. AAC 1 with the highest activator concentration has the greatest strength due to higher reaction rate and the formation of a less porous matrix [3,4]. For example, the 28-day compressive strength of AAC 1 (0% activator dilution) and AAC 3 (7.76% activator dilution) was 58.3 MPa and 51.4 MPa respectively, under wet curing (Fig. 8). The compressive strength of mortars AAMs and PCM shows a similar trend to their corresponding concrete mixes.

The compressive strength of AAC and PCC decreases after prolonged exposure to both accelerated and natural CO_2. For example, the compressive strength of AAC 1 and PCC under accelerated CO_2 exposure after 2113days is 56.5 MPa and 36.5 MPa respectively, it is 57.2 MPa and 42.5 MPa under natural CO_2 exposure. These values are lower than the standard 28days compressive strengths of 58.3 MPa and 50.1 MPa for AAC 1 and PCC respectively. These results suggest the decalcification of C-A-S-H and C–S–H gel in both concrete types at higher CO_2 concentration over a prolonged duration results in lower compressive strength. Similar findings are presented by Yubin et al. [40], Song et al. [41] and Behfarnia et al. [42], showing significant reduction in the compressive strength of GBFS-based concrete when exposed to accelerated 3%–5% CO_2 concentrations.

There is a moderate reduction in compressive strength of AAC and PCC under natural CO_2 exposure. AAC and PCC cured under natural CO_2 concentrations have higher compressive strength than under high CO_2 concentrations as seen in Fig. 8. Nedeljkovic' et al. [43] and Robayo-Salazar et al. [8] reported that the compressive strength of GBFS-based AAM is moderately reduced after 48 weeks exposure to 1% CO_2 concentration. This was attributed to densification by carbonate precipitates within the pore structure of concrete. There will be filler effect within the concrete pore structure [44] and higher strength than the decalcified concrete exposed to accelerated CO_2 concentration.

3.2.2. Intrudable porosity

The relationship between intrudable porosity and compressive strength of AAC and PCC exposed to accelerated and natural CO_2 concentration at 2113days is shown in Fig. 9. It shows the impact of carbonation on porosity and compressive strength. A cluster of points indicating the relationship between porosity and compressive strength for AAC represent porosity between 8% and 18% corresponding to compressive strengths between 58 MPa and 38 MPa. PCC shows highest porosity of 31% and lowest compressive strength of 36 MPa.

As expected, the porosity of both AAC and PCC is synonymous with their compressive strength. AAC having higher compressive strength than PCC shows lower intrudable porosity (Fig. 9). It is also observed that AAC and PCC exposed to accelerated carbonation have lower compressive strength with higher intrudable porosity compared with samples exposed to natural carbonation. A kinetically stable sodium carbonate is produced when AAC is exposed to natural CO_2 while a more unstable bicarbonate is produced when exposed to accelerated CO_2 concentration [31]. This relative kinetic stability of carbonates and bicarbonates influences the pore structure of AAC. The greater amount of unstable bicarbonate produced in AAC under accelerated carbonation results in higher intrudable porosity as shown in Fig. 9.

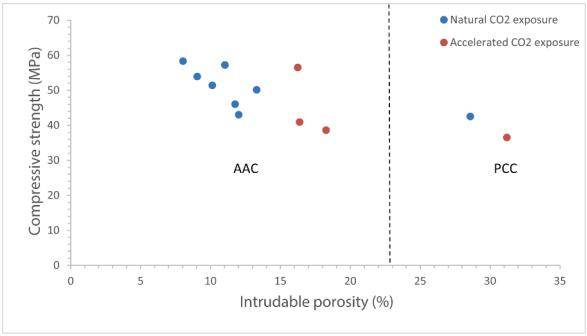

Fig. 9. Relationship between porosity and compressive strength of AAC and PCC under natural and accelerated CO_2 exposure, after 2113days.

Concrete diffusivity which is a function of porosity is a major controlling factor for carbonation [24]. The ingress of CO_2 and moisture from the environment into AAC is inhibited by decreasing porosity. For example, AAC 1 has the lowest porosity of 16.24%, followed by AAC 2 and 3 which had 16.37% and 18.27% porosity respectively at 2113 days of accelerated CO_2 exposure. Their corresponding depth of carbonation, discussed in section 3.3.1, follows the same trend. The carbonation process is complex because it involves the transport of liquid and gas, which cannot be represented simply with Fick's law of diffusion [45]. Lagerblad [46] observed that the difficulty in applying Fick's law is due to simultaneous inward and outward diffusion of carbonate and calcium ions respectively. The pore structure is altered during the carbonation process involving carbonate and calcium ions. For AAC under natural carbonation exposure, a pore structure evolves as the outward diffusion of $CaCO_3$ forms stable precipitates that block the concrete pores [47]. However, in PCC, the calcium ions disintegrate by a process of decalcification and diffuse outward into the environment. Larger pores evolve during the decalcification of C–S–H in PCC and reduce its strength and increase its porosity unlike the precipitation of $CaCO_3$ in AAC which increases its strength and reduces porosity (Fig. 9). The blocking of pores by $CaCO_3$ in AAC and the enlarging of pores in PCC by disintegration of calcium ions due to decalcification, under natural carbonation, was also reported by Palacios et al. [48].

Under accelerated carbonation, bicarbonate is formed in AAC (Fig. 4). It has a lower molar volume which reduces the pore blocking effect and allows more ingress of CO_2, unlike the pore blocking effect of carbonate under natural CO_2 exposure [31]. Fig. 10 shows the decalcification products on the surface of AAC under accelerated carbonation only. However, PCC does not have decalcification products on sample surfaces exposed to accelerated and natural carbonation.

3.2.3. *Carbonation depth*

The carbonated and non-carbonated zones identified by the phenolphthalein test are marked on the broken faces of both AAC and PCC in Fig. 11. This shows that the carbonation front occurred at the two opposite faces of specimens exposed to CO_2 while the other two opposite faces coated with bitumen paint show insignificant carbonation front. The results in Figs. 11 and 6 (section 3.1.3) indicate that carbonation of AAC samples had occurred at pH considerably greater than 9 which is the threshold for carbonation in PCC. The likely reason is lower calcium oxide content in AAC (Table 4, section 3.1.2), but not loss of its alkalinity which is boosted by higher content of other alkalis (Na^+, K^+, Al^{3+} and Mg^{2+}). The summation of Na^+, K^+, Al^{3+} and Mg^{2+} contents in AAC 1, 2, 3 are 6.5%, 6.4%, 5.9% compared with 1.2% for PCC (Table 4, section 3.2.1). These alkalis are present in AAC in substantial amount thus boosting its pH by replacing Ca^{2+} in the negative surface charge of the silicate chain. Fig. 12 shows a direct relationship between the depleted CaO content (difference% in Table 3) and depth of carbonation with a high correlation of 0.93. This shows the strong impact of Ca^{2+} depletion, rather than alkali content, in AAC and PCC in influencing the depth of carbonation measured by the phenolphthalein indicator method.

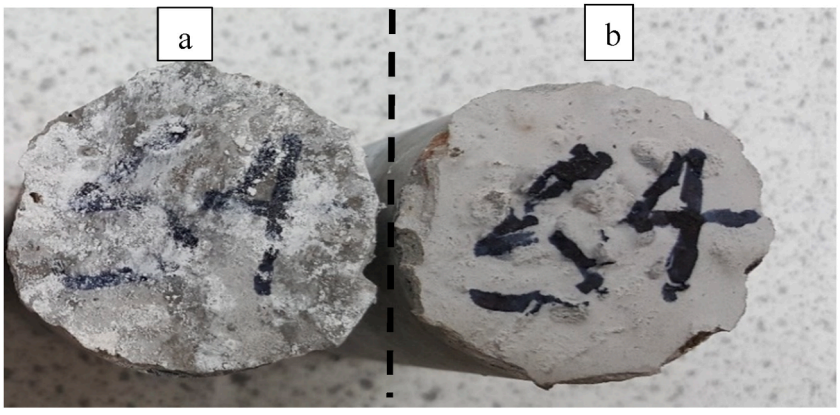

Fig. 10. Showing (a) accelerated CO_2 exposure of AAC and (b) natural CO_2 exposure of AAC.

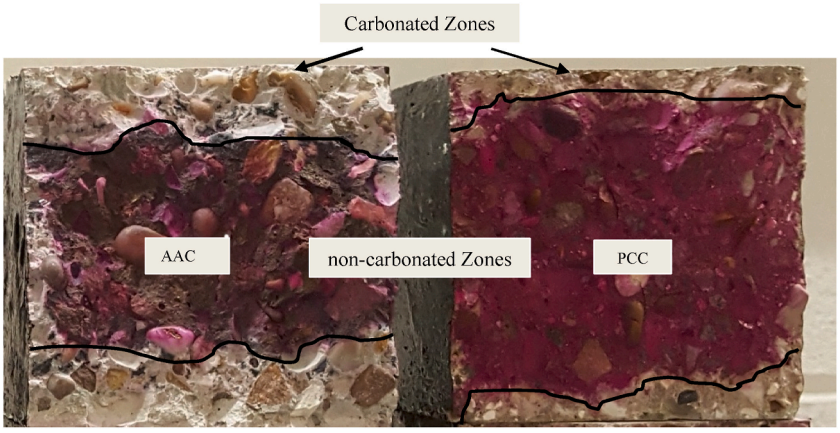

Fig. 11. Phenolphthalein-sprayed faces of AAC and PCC after 327days of CO_2 exposure.

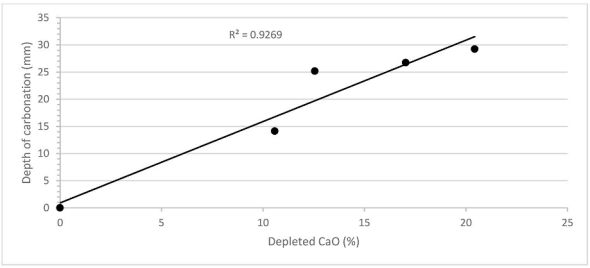

Fig. 12. Relationship between depleted CaO and carbonation depth at 327days CO_2 exposure.

The depths of carbonation in AAC and PCC were determined up to 2113 days exposure at 5% CO_2 concentration, 60 ± 5% R.H. and 20 ± 2 °C for the accelerated condition and 0.04% CO_2 concentration, 60 ± 5% R.H. and 20 ± 2 °C for the natural (ambient) condition. The results are shown in Fig. 13.

Fig. 13 shows the rate of carbonation in AAC 1, 2, 3 and PCC under accelerated and natural exposures, given by the phenolphthalein indicator test method [11]. The carbonation profile of AAC shows a higher rate of carbonation than PCC in Fig. 13 for the accelerated exposure. The average carbonation depth in AAC 1, 2 and 3 is 32.6 mm, 34.8 mm and 36.01 mm respectively while it is 28.5 mm for PCC after 2113 days of accelerated CO_2 exposure (Fig. 13). Other authors [48–50] also observed similar increase in the depth of carbonation for water-glass activated slag concrete relative to PCC under accelerated CO_2 exposure. Their specimens were cured in a closed chamber containing K_2CO_3 solution, kept at a relative humidity of 43.2%. The chamber was saturated with CO_2 twice daily with unknown concentration of the CO_2.

Conversely, in Fig. 13, the carbonation depth under natural CO_2 exposure shows quite the opposite result with PCC having the highest carbonation depth than AAC. The carbonation depths in AAC 1, 2, 3 and PCC are 21.4 mm, 21.7 mm, 23.2 mm and 25.7 mm respectively after 2113 days of natural CO_2 exposure (Fig. 13). The natural CO_2 exposure of AAC does not produce bicarbonates unlike when it is subjected to accelerated CO_2 exposure [31]. The apparent impact of bicarbonates is a higher carbonated depth in AAC under accelerated exposure to 5% CO_2 concentration as shown in Fig. 13. For example, AAC 1 has a carbonated depth of 32.6 mm and 21.4 mm when exposed to 2113 days of accelerated and natural CO_2 concentrations respectively. For PCC, there is no significant difference in carbonation depths when exposed to either accelerated (28.5 mm) or natural (25.7 mm) carbonation. The small difference in the carbonation depths of PCC under accelerated (5% CO_2 concentration) and natural (< 0.1% CO_2 concentration) can be attributed to differences in their CO_2 concentrations rather than the impact of CO_2 on their pore chemistry [6].

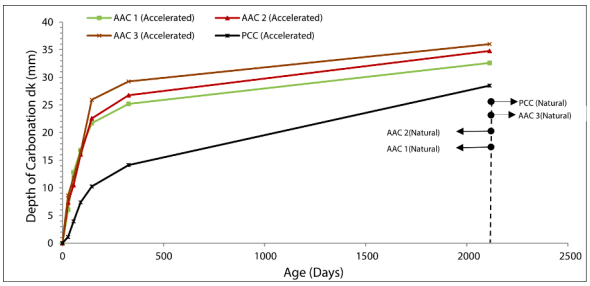

Fig. 13. Depth of carbonation in AAC and PCC up to 2113days exposure.

A steep increase in depth of carbonation occurs in the AAC samples within 145 days of accelerated CO_2 exposure in the chamber (Fig. 13). Bernal et al. [31] identified the formation of sodium carbonate to be responsible for the early stage of carbonation in AAC. The authors [31] attributed the low relative humidity within the AAC matrix at this early stage to facilitate carbonation of geopolymer products which are in contact with water vapour (lower humidity) rather than liquid. This forms a kinetically stable sodium carbonate which slowly converts to bicarbonates at later stages of accelerated CO_2 exposure. This explanation is supported by the sodium bicarbonate by-products observed in the carbonated samples of AAC 1, 2 and 3 in section 3.1.1. Nahoclite ($NaHCO_3$) is the bicarbonate product observed in AAC after 2113days exposure to 5% CO_2 concentration at 60 ± 5% R.H and 20 ± 2 °C (Fig. 5). This phenomenon does not apply under natural CO_2 concentration. At natural CO_2 exposure, the stable sodium carbonate did not convert to sodium bicarbonate by-products in AAC.

However, this is not the case in PCC (Fig. 13) where the early rate of increase in carbonation depth, and the depth at 145 days are much lower. Exposure of PCC under higher CO_2 concentration accelerates the carbonation process without changing its reaction kinetics, unlike AAC where there is a change in reaction kinetics. Therefore, the accelerated carbonation test method used for PCC [6] is unsuitable for AAC to predict its long-term resistance to carbonation. AAC offers better carbonation resistance than a similar grade of PCC for field applications exposed to natural conditions.

3.2.4. Carbonation and drying shrinkage

The total shrinkage (Dt) of specimens exposed in the carbonation chamber at 5% CO_2 concentration, 60 ± **5**% R.H. and a temperature of 20 ± 2 °C is plotted in Fig. 14. The corresponding drying shrinkage (Dd) of specimens exposed in the laboratory air at 60 ± **5**% R.H. and a temperature of 20 ± 2 °C is also plotted in Fig. 14. The absolute carbonation shrinkage (Dc) of these specimens is the difference between the total shrinkage (Dt) and drying shrinkage (Dd) as shown in equation (1).

$$Dc = Dt - Dd \quad 1$$

where.

Dc = absolute carbonation shrinkage
Dt = total shrinkage of specimens exposed in carbonation chamber at 5% CO_2 concentration, 20 ± 2^0C and *60 ± 5% R.H*
Dd = Drying shrinkage of specimens exposed in the laboratory air at 0.4% CO_2 concentration, 20 ± 2 °C and 60 ± 5% R.H.

The shrinkage reducing admixture (SRA) enhances workability while the retarder (R42) increases the setting time of AAC concrete and mortars. These admixtures were required for the AAC mixes at the activator/binder ratio of 0.47 (Table 1). The workability and setting time of PC concrete mixes was satisfactory at water/cement ratio of 0.47 (Table 1) and did not require SRA and R42.

The total shrinkage (Dt) under CO_2 exposure is higher than the drying shrinkage (Dd) in both AAC and PCC. The (Dt) strain at 50 days is 429 με, 576 με and 311 με for AAC 1, 3 and PCC respectively. The corresponding (Dd) strain is 418 με, 526 με and 270 με respectively. The total shrinkage (Dt) is higher than the drying shrinkage (Dd) since it combines the shrinkage caused by drying (Dd) and absolute carbonation (Dc). The absolute carbonation shrinkage is influenced by the decomposition of the binder products, mainly Ca(OH) and C(N)-A-S-H, under CO_2 exposure [51]. However, the true value of absolute carbonation shrinkage (Dc) may not be as straightforward due to combination of the two distinctive processes of carbonation and drying involved in the total shrinkage (Dt) data and the interaction of these processes being different for AAC and PCC.

The absolute carbonation shrinkage (Dc) is influenced by porosity. For example, AAC 1 which has the lowest (negligible) absolute carbonation shrinkage of 11 με (429 με minus 418 με) at 50days age also has the lowest 28-day porosity of 8.03% (Fig. 10). AAC 3 and PCC have higher porosities of about 10.1 and 13.3% respectively (Fig. 10) and their absolute carbonation shrinkage (Dc) is greater at 50 με and 41 με respectively at 50days.

4. Conclusions

This paper presents the chemical and mineralogical characteristics of AAC and AAM determined by EDS, XRF, XRD and pH analysis under accelerated and natural carbonation. Tests were conducted on the carbonated and non-carbonated zones determined by the

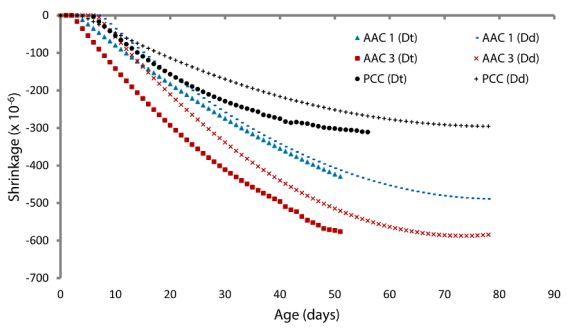

Fig. 14. Total and drying shrinkage of AAC and PCC with age.

phenolphthalein indicator method. Studies on the carbonation rates, shrinkage (drying, carbonation), porosity and compressive strength over long-term exposure (up to 2113 days) were also carried out. The following conclusions can be drawn from the study.

1. Carbonation causes greater depletion of Ca^{2+} in AAC than PCC primarily because AAC has lesser Ca^{2+} than PCC in its hydration products. For example, the depletion of Ca^{2+} is 12.55%, 17.03%, 20.43% for AAC 1, 2, 3 respectively and 10.58% for PCC. However, the content of other alkalis such as Na^{2+}, K^{+} and Mg^{2+} is much greater in AAC and they account for the higher pH in AAC than PCC both in their "carbonated" and "non-carbonated" states. The total alkali content in the "carbonated" samples of AAC 1 (19.3%, pH 10.46) and AAC 2 (18.5%, pH 10.37) is higher than the control PCC (15.3%, pH 9.56). Similarly, the total alkali content in the "non-carbonated" samples of AAC 1 is higher than the control PCC. The alkalinity of AAM is affected similarly as AAC by carbonation except the additional alkalinity provided by the coarse aggregate to AAC. The pH of carbonated AAM 1 (10.02), AAM 2 (10.1) and AAM 3 (10.05) is much higher than PCM (8.69).
2. The phenolphthalein indicator test gives deeper depths of carbonation in AAC than PCC. However, the pH of the "carbonated" zones defined by this test in AAC significantly exceeds the carbonation defining pH limit of 9. The phenolphthalein test and pH values in AAC provide contrary evidence of carbonation unlike the control PCC which has a pH below 9 (non-alkaline) in its "carbonation" zone. The phenolphthalein test indicates the depletion of alkali Ca^{+2} under carbonation, which is the predominant alkali in PCC, and detects its carbonation depth accurately. The phenolphthalein test overestimates the carbonation of AAC which, although low in Ca^{+2}, is richer in other alkalis (Na^{+}, K^{+}, Al^{3+} and Mg^{2+}).
3. A strong ($R^2 = 0.93$) linear relationship exists between the CaO% depletion caused by carbonation and the carbonation depth of AAC and PCC. This shows the strong impact of Ca^{2+} depletion on the depth of carbonation measured by the phenolphthalein test.
4. The carbonation depth of AAC under natural CO_2 exposure is lower than a similar grade of PCC. However, under accelerated carbonation at high CO_2 concentration, the depth of carbonation is higher in AAC. The accelerated carbonation reaction in AAC changes, also producing bicarbonates ($NaHCO_3$), resulting in greater carbonation depths. This reaction is similar in alkali activated mortars.
5. The release of alkali content from the coarse aggregate increases the pH of both AAC and PCC. For example, the pH of AAC and PCC is 10.25 and 9.56 respectively and their corresponding mortars are 10.05 and 8.69. Also, the pH of AAC and AAM decreases with the reduction of molarity of its alkali activator.
6. AAC and PC samples exposed to natural carbonation have higher compressive strength than those exposed to accelerated carbonation. For example, the compressive strength of AAC 1 and PCC after 2113days of accelerated carbonation is 56.5 MPa and 36.5 MPa respectively, it is 57.2 MPa and 42.5 MPa under natural CO_2 exposure. Longer duration of carbonation reduces the compressive strength of both AAC and PCC due to an increase in their porosity.
7. The 28day compressive strength of AAC and AAM is influenced by porosity which decreases with increasing molarity of activator. For example, the 28day compressive strength of AAM 1, AAM 2 and AAM 3 are 55.5 MPa, 51.3 MPa and 46.4 MPa respectively. Similarly, the 28day compressive strength of AAC 1, AAC 2 and AAC 3 are 58.3 MPa, 53.9 MPa and 51.4 MPa respectively.
8. Accelerated carbonation in AAC under high CO_2 exposure starts by the rapid formation of sodium carbonate which converts to bicarbonate at later stages. These reactions do not occur under natural CO_2 exposure where carbonates do not convert to bicarbonate. Exposure of PCC under high CO_2 concentration accelerates carbonation without changing its reaction kinetics, unlike AAC where a change in the reaction kinetics results in higher carbonation than under natural CO_2 exposure.
9. The total shrinkage (Dt) comprising of shrinkage components of drying (Dd) and carbonation (Dc) in AAC is greater than PCC. The absolute carbonation shrinkage (Dc) is much lower than drying shrinkage (Dd) in both AAC and PCC. For example, absolute carbonation shrinkage (Dc) for AAC 1, 3 and PCC is 11$\mu\epsilon$, 50$\mu\epsilon$ and 41$\mu\epsilon$ respectively and their corresponding drying shrinkage (Dd) is 418$\mu\epsilon$, 526$\mu\epsilon$ and 270$\mu\epsilon$ at 50days.

Authors statement

Olalekan O. Ojedokun and P.S. Mangat participated in the conceptualization of Ideas; formulation and evolution of overarching research goals and aims. Both authors agreed on the development and the design of methodology, creation of models. Olalekan O. Ojedokun contributed to the utilization of software. P.S. Mangat carried out the validation and verification of the overall replication and reproductivity of results and other research outputs. The application of statistical tools and other formal techniques to analyze study data was carried out by Olalekan O. Ojedokun. Both authors conducted the research and investigation process while Olalekan O. Ojedokun specifically performed the experiments and data collection. The initial draft was written by Olalekan O. Ojedokun while the review, editing and the final presentation of the published work was carried out by both authors. P.S. Mangat carried out the critical review, commentary and revisions which include the pre and post publication stages. The supervision, oversight and leadership responsibilities were performed by P.S. Mangat. Funding acquisition of financial support for the project leading to this publication was carried out by both authors.

Declaration of competing interest

The authors declare that they have no known competing financial interests or personal relationships that could have appeared to influence the work reported in this paper.

Data availability

The data that has been used is confidential.

Acknowledgment

The authors gratefully acknowledge the support of the Materials and Engineering Research Institute at Sheffield Hallam University, United Kingdom; Tertiary Education Trust Fund, Federal Republic of Nigeria; Innovate UK, United Kingdom; EPSRC, United Kingdom.

References

[1] I. Bianco, B. Ap Dafydd Tomos, R. Vinai, Analysis of the environmental impacts of alkali-activated concrete produced with waste glass-derived silicate activator – a LCA study, J. Clean. Prod. 316 (2021) 128383, https://doi.org/10.1016/j.jclepro.2021.128383.
[2] A. Alsalman, L.N. Assi, R.S. Kareem, K. Carter, P. Ziehl, Energy and CO2 emission assessments of alkali-activated concrete and Ordinary Portland Cement concrete: a comparative analysis of different grades of concrete, Clean. Environ. Syst. 3 (2021) 100047, https://doi.org/10.1016/j.cesys.2021.100047.
[3] P.S. Mangat, O.O. Ojedokun, Influence of curing on pore properties and strength of alkali activated mortars, Construct. Build. Mater. 188 (2018) 337–348, https://doi.org/10.1016/J.CONBUILDMAT.2018.07.180.
[4] O.O. Ojedokun, P.S. Mangat, Characterization and pore structure of rice husk ash cementitious materials, in: Am. Concr. Institute, ACI Spec. Publ., 2018.
[5] P.S. Mangat, O.O. Ojedokun, Free and bound chloride relationships affecting reinforcement cover in alkali activated concrete, Cem. Concr. Compos. (2020) 103692, https://doi.org/10.1016/j.cemconcomp.2020.103692.
[6] John L. Provis, J.S.J. van Deventer, Alkali-Activated Materials State-Of-The-Art Report, RILEM TC 224-AAM, 2014.
[7] P.S. Mangat, O.O. Ojedokun, P. Lambert, Chloride-initiated corrosion in alkali activated reinforced concrete, Cem. Concr. Compos. 115 (2021), https://doi.org/10.1016/j.cemconcomp.2020.103823.
[8] R.A. Robayo-Salazar, A.M. Aguirre-Guerrero, R. Mejía de Gutiérrez, Carbonation-induced corrosion of alkali-activated binary concrete based on natural volcanic pozzolan, Construct. Build. Mater. (2020), https://doi.org/10.1016/j.conbuildmat.2019.117189.
[9] M. Cyr, R. Pouhet, Carbonation in the pore solution of metakaolin-based geopolymer, Cement Concr. Res. (2016), https://doi.org/10.1016/j.cemconres.2016.05.008.
[10] A. Buchwald, M. Vanooteghem, E. Gruyaert, H. Hilbig, N. De Belie, Purdocement: application of alkali-activated slag cement in Belgium in the 1950s, Mater. Struct. Constr. 48 (2015) 501–511, https://doi.org/10.1617/S11527-013-0200-8.
[11] BS EN 14630, Products and Systems for the Protection and Repair of Concrete Structures — Test Methods — Determination of Carbonation Depth in Hardened Concrete by the Phenolphthalein Method, 2006.
[12] PAS 8820: 2016, Construction materials : Alkali-activated cementitious material and concrete : specification., BSI Standards, n.d. https://shop.bsigroup.com/ProductDetail?pid=000000000030318035 (accessed September 17, 2018)..
[13] X. Xie, H. Wei, X. Zuo, D. Cui, Effect of carbonation on microstructure evolution of alkali-activated slag pastes, Key Eng. Mater. 929 (2022) 201–212, https://doi.org/10.4028/P-HP6T1T.
[14] I. Galan, C. Andrade, M. Castellote, Natural and accelerated CO2 binding kinetics in cement paste at different relative humidities, Cement Concr. Res. 49 (2013) 21–28, https://doi.org/10.1016/J.CEMCONRES.2013.03.009.
[15] S.A. Bernal, J.L. Provis, D.G. Brice, A. Kilcullen, P. Duxson, J.S.J. Van Deventer, Accelerated carbonation testing of alkali-activated binders significantly underestimates service life: the role of pore solution chemistry, Cement Concr. Res. 42 (2012) 1317–1326, https://doi.org/10.1016/j.cemconres.2012.07.002.
[16] T. Bakharev, J.G. Sanjayan, Y.-B. Cheng, Resistance of alkali-activated slag concrete to carbonation, Cement Concr. Res. 31 (2001) 1277–1283.
[17] S.A. Bernal, R. San Nicolas, J.L. Provis, R. Mejía De Gutiérrez, J.S.J. Van Deventer, Natural carbonation of aged alkali-activated slag concretes, Mater. Struct. Constr. 47 (2014) 693–707, https://doi.org/10.1617/S11527-013-0089-2/FIGURES/12.
[18] S.A. Bernal, X. Ke, M. Criado, S. Mundra, J.L. Provis, SP-XXX-1 Factors controlling carbonation resistance of alkali-activated materials, in: Proc. 10th ACI/RILEM Int. Conf. Cem. Mater. Altern, Bind. Sustain. Concr., 2017, pp. 1–36.
[19] O. Ojedokun, Durability properties of an alkali activated cementitious material, http://shura.shu.ac.uk/21933/, 2018. (Accessed 23 June 2020).
[20] G.J.G. Gluth, K. Arbi, S.A. Bernal, D. Bondar, A. Castel, S. Chithiraputhiran, A. Dehghan, K. Dombrowski-Daube, A. Dubey, V. Ducman, K. Peterson, P. Pipilikaki, S.L.A. Valcke, G. Ye, Y. Zuo, J.L. Provis, RILEM TC 247-DTA round robin test: carbonation and chloride penetration testing of alkali-activated concretes, Mater. Struct. Constr. (2020), https://doi.org/10.1617/s11527-020-1449-3.
[21] F. Ren, X. Chen, Q. Zeng, C. Zhou, Effects of pure carbonation on pore structure and water permeability of white cement mortars, CEMENT 9 (2022) 100040, https://doi.org/10.1016/j.cement.2022.100040.
[22] C. Lu, Z. Zhang, C. Shi, N. Li, D. Jiao, Q. Yuan, Rheology of alkali-activated materials: a review, Cem. Concr. Compos. 121 (2021) 104061, https://doi.org/10.1016/j.cemconcomp.2021.104061.
[23] O. O, P.S. Mangat, Ojedokun, Bound chloride ingress in alkali activated concrete, Construct. Build. Mater. 212 (2019) 375–387, https://doi.org/10.1016/j.conbuildmat.2019.03.302.
[24] A.M. Neville, Properties of Concrete, Pearson Education Limited, 2011.
[25] British standards institution, concrete — specification , performance , production and conformity, BS (Breed. Sci.) 206 (2016).
[26] British Standards Institution, Testing Hardened Concrete Part 210: Determination of the Potential Carbonation Resistance of Concrete – Accelerated Carbonation Method, 2013.
[27] British Standards Institution, BS EN 12390-16:2019 Testing hardened concrete Determination of the shrinkage of concrete - European Standards, (n.d.). https://www.en-standard.eu/bs-en-12390-16-2019-testing-hardened-concrete-determination-of-the-shrinkage-of-concrete/(accessed March 1, 2023)..
[28] G. Plusquellec, M.R. Geiker, J. Lindgard, J. Duchesne, B. Fournier, K. De Weerdt, Determination of the pH and the free alkali metal content in the pore solution of concrete: review and experimental comparison, Cement Concr. Res. 96 (2017) 13–26, https://doi.org/10.1016/j.cemconres.2017.03.002.
[29] BS EN 12390-3:2009, Testing Hardened Concrete Part 3: Compressive Strength of Test Specimens, 2009.
[30] BS EN 12390-7:2009, Testing hardened concrete. Density of hardened concrete – BSI British Standards, in: n.d. https://shop.bsigroup.com/ProductDetail/?pid=000000000030164912 (accessed June 21, 2018)..
[31] S.A. Bernal, J.L. Provis, B. Walkley, R. San Nicolas, J.D. Gehman, D.G. Brice, A.R. Kilcullen, P. Duxson, J.S.J. Van Deventer, Gel nanostructure in alkali-activated binders based on slag and fly ash, and effects of accelerated carbonation, Cement Concr. Res. (2013), https://doi.org/10.1016/j.cemconres.2013.06.007.
[32] Y. Ma, W. Li, M. Jin, J. Liu, J. Zhang, J. Huang, C. Lu, H. Zeng, J. Wang, H. Zhao, J. Tang, Influences of leaching on the composition, structure and morphology of calcium silicate hydrate (C–S–H) with different Ca/Si ratios, J. Build. Eng. 58 (2022) 105017, https://doi.org/10.1016/j.jobe.2022.105017.
[33] H. Ye, A. Radlińska, J. Neves, Drying and carbonation shrinkage of cement paste containing alkalis, Mater. Struct. (2017), https://doi.org/10.1617/s11527-017-1006-x.
[34] G. Huang, K. Yang, Y. Sun, Z. Lu, X. Zhang, L. Zuo, Y. Feng, R. Qian, Y. Qi, Y. Ji, Z. Xu, Influence of NaOH content on the alkali conversion mechanism in MSWI bottom ash alkali-activated mortars, Construct. Build. Mater. 248 (2020) 118582, https://doi.org/10.1016/j.conbuildmat.2020.118582.
[35] S.R. Paudel, M. Yang, Z. Gao, pH level of pore solution in alkali-activated fly-ash geopolymer concrete and its effect on ASR of aggregates with different silicate contents, J. Mater. Civ. Eng. 32 (2020) 04020257, https://doi.org/10.1061/(ASCE)MT.1943-5533.0003344.
[36] X. Dai, S. Aydın, M.Y. Yardımcı, K. Lesage, G. De Schutter, Effects of activator properties and GGBFS/FA ratio on the structural build-up and rheology of AAC,

Cement Concr. Res. 138 (2020) 106253, https://doi.org/10.1016/j.cemconres.2020.106253.
[37] S. Mundra, S.A. Bernal, M. Criado, P. Hlaváček, G. Ebell, S. Reinemann, G.J.G. Gluth, J. Provis, Steel corrosion in reinforced alkali-activated materials, RILEM Tech. Lett. (2017), https://doi.org/10.21809/rilemtechlett.2017.39.
[38] K. Pasupathy, M. Berndt, A. Castel, J. Sanjayan, R. Pathmanathan, Carbonation of a blended slag-fly ash geopolymer concrete in field conditions after 8 years, Construct. Build. Mater. 125 (2016) 661–669, https://doi.org/10.1016/J.CONBUILDMAT.2016.08.078.
[39] Y. Qin, H. Yang, Carbonation dominates the acid intake of recycled concrete aggregate subjected to intermittent leaching, Construct. Build. Mater. 89 (2015) 110–114, https://doi.org/10.1016/j.conbuildmat.2015.04.038.
[40] Y. Jun, S.H. Han, J.H. Kim, Performance of CO2-cured alkali-activated slag pastes during curing and exposure, Int. J. Concr. Struct. Mater. 17 (2023) 1–11, https://doi.org/10.1186/S40069-022-00563-3/FIGURES/6.
[41] K.-I. Song, J.-K. Song, B.Y. Lee, K.-H. Yang, Carbonation characteristics of alkali-activated blast-furnace slag mortar, Adv. Mater. Sci. Eng. 2014 (2014) 326458, https://doi.org/10.1155/2014/326458.
[42] K. Behfarnia, M. Rostami, An assessment on parameters affecting the carbonation of alkali-activated slag concrete, J. Clean. Prod. 157 (2017) 1–9, https://doi.org/10.1016/j.jclepro.2017.04.097.
[43] M. Nedeljković, Y. Zuo, K. Arbi, G. Ye, Carbonation resistance of alkali-activated slag under natural and accelerated conditions, J. Sustain. Metall. 4 (2018) 33–49, https://doi.org/10.1007/s40831-018-0166-4.
[44] A. Aboulayt, M. Riahi, M. Ouazzani Touhami, H. Hannache, M. Gomina, R. Moussa, Properties of metakaolin based geopolymer incorporating calcium carbonate, Adv. Powder Technol. 28 (2017) 2393–2401, https://doi.org/10.1016/j.apt.2017.06.022.
[45] R. Collepardi, M, A. Marcialis, Turrizuani, The kinetics of chloride ions penetration in concrete, II Cem 67 (1970) 157–164.
[46] B. Lagerblad, Carbon Dioxide Uptake during Concrete Life Cycle – State of the Art, 2005.
[47] F. Puertas, M. Palacios, T. Vázquez, Carbonation process of alkali-activated slag mortars, J. Mater. Sci. (2006), https://doi.org/10.1007/s10853-005-1821-2.
[48] M. Palacios, F. Puertas, Effect of carbonation on alkali-activated slag paste, J. Am. Ceram. Soc. 89 (2006) 3211–3221, https://doi.org/10.1111/j.1551-2916.2006.01214.x.
[49] R. Xu, H. Wang, Q. Zha, J. Lin, Improving the carbonation resistance of alkali-activated slag mortars with different additives: experimental evaluations, Construct. Build. Mater. 366 (2023) 130197, https://doi.org/10.1016/j.conbuildmat.2022.130197.
[50] M.A.T. Marple, B. Koroglu, K. Morrison, J. Crowhurst, A. Balachandra, P. Soroushian, H.E. Mason, Accelerated carbonation and structural transformation of blast furnace slag by mechanochemical alkali-activation, Cement Concr. Res. 156 (2022) 106760, https://doi.org/10.1016/j.cemconres.2022.106760.
[51] M. Nedeljković, Y. Zuo, K. Arbi, G. Ye, Carbonation resistance of alkali-activated slag under natural and accelerated conditions, J. Sustain. Metall. 4 (2018) 33–49, https://doi.org/10.1007/S40831-018-0166-4/FIGURES/16.